Aeroservoelastic Design Optimization of a Flexible Wing

Sohrab Haghighat *, Joaquim R. R. A. Martins †, Hugh H. T. Liu‡

In this paper a multidisciplinary design optimization framework is developed that integrates control system design with aerostructural design. The equations of motion are derived for a flexible aircraft and used to perform aeroservoelastic analysis. The objective of this framework is to go beyond the current limits of aircraft performance through simultaneous design optimization of aerodynamic shape, structural sizing and control system. The control system uses load alleviation to reduce the critical structural loads. Time-domain analysis of the aircraft performing an altitude change maneuver and encountering an atmospheric gust is included in the design process. The optimal trade-off between aerodynamics, structures and control system is found by maximizing the endurance subjected to stress and maneuverability constraints. Two cases — with and without load alleviation system — are considered. Due to the proposed MDO framework, the inclusion of load alleviation system in design leads to a significant increase in endurance performance.

I. Introduction

With the advent of multidisciplinary design optimization (MDO) techniques, designers have started to integrate various disciplines in the aircraft design process. The strong coupling between aerodynamics and structures has motivated aircraft designers to apply MDO techniques to aerostructural design problems. Previous work in this area has focused on minimizing the total drag or maximizing the aircraft range by simultaneously optimizing the structural and aerodynamic design variables [1, 2, 3]. In order to improve aircraft efficiency, researchers have also investigated nonplanar lifting surface configurations, where aerostructural optimization are performed to find optimal configurations, such as C-wings, joined wings, and winglets [4, 5]. In all these efforts, the aircraft structures are designed to have optimum cruise performance while withstanding the critical loads corresponding to other flight conditions.

Through the use of multiple control surfaces, active aeroelastic wing technology can be exploited to reduce the wing loading during a flight maneuver [6, 7, 8, 9, 10]. More than 25 years of extensive research in the field of aeroservoelasticity has shown that aeroservoelastic analysis and design should be considered as early as possible in the aircraft design process [11, 12]. One of the earliest works in the field of aeroservoelastic optimization was performed by Suzuki [7], who minimized wing structural weight by designing the structure and control system simultaneously. Control stability and maximum stress due to an atmospheric gust were the design constraints used in this optimization work. Aerodynamic design, however, was not considered in this work and the aircraft planform was kept unchanged. An aeroservoelastic design framework was also presented by Idan *et al.* [13], where the interaction between the aircraft structure and control system was considered. First, a preliminary structural and control optimization was performed separately. The resulting structure and control system were then optimized considering closed-loop control margins and flutter. The same framework was later used to perform simultaneous structural and control optimization in the presence of parameter uncertainty [14].

Zink *et al.* addressed the design of structural parameters and gear ratios of a lightweight fighter performing symmetric and antisymmetric (rolling) maneuvers [15]. The optimization formulation was based on static aeroelastic equations. The integrated approach results were compared to those obtained using a sequential approach; the former was shown to be more effective and converged to a lower structural weight. The same authors also considered maneuver load inaccuracies and their effects on the optimum design [16].

The development of a detailed mathematical model that can integrate flight dynamics with structures and aerodynamics is essential in active aeroelastic wing design. Some of the work that addressed the active aeroelastic wing design adopted quasi-steady flight models, where structural deflections are assumed to have reached their steady-state conditions [17, 15, 18]. Mathematical formulations of flexible aircraft flight dynamics are mainly based on one of two approaches: the *mean-axes* method, or the *quasi-coordinate* method. Waszak and Schmidt [19] and Schmidt and Raney [20] developed the equations of motion for a flexible aircraft using the mean-axes method. The use of simple aerodynamic strip theory and the small structural deflections assumption are the main limitations of this formulation. Formulations using the quasi-coordinate method, where the axes are fixed to a specific point of the aircraft, have also

*Ph.D. Candidate, University of Toronto Institute for Aerospace Studies, Student Member AIAA
†Associate Professor, University of Michigan, Department of Aerospace Engineering, Senior Member AIAA
‡Associate Professor, University of Toronto Institute for Aerospace Studies, Senior Member AIAA

been developed [21, 22, 23, 24, 25]. In this work, the mathematical formulations of aircraft flight dynamics is based on the quasi-coordinate method. Several models have been used to evaluate the aerodynamic forces and moments of a flexible aircraft. However, most researchers so far have used the aerodynamic strip theory.

In addition to different approaches used to represent flexible aircraft, different design objectives have also been considered by the researchers. The Previous work on aeroservoelastic synthesis has focused either on achieving the required maneuverability or on designing lighter wings by utilizing load alleviation. However, aeroservoelasticity can also be used to optimize the overall performance of an aircraft by minimizing an objective function, such as endurance, range, or fuel consumption. Also, the design variables used in previous work have mostly been limited to structural and control system parameters, while the aerodynamic shape has been kept constant during optimization. Nam *et al.* [8] conducted one of the few investigations that considered integrated planform and control system design.

Since simultaneous optimization yields better results than those obtained through performing sequential optimization [26, 15, 27], the real potential of including aeroservoelastic synthesis in the aircraft design process can only be realized with a simultaneous optimization approach. In a traditional design process, the aircraft configuration is designed first, and the control system is designed second. This traditional approach prevents the flight control system from affecting the aircraft configuration. It has been shown that by designing the aircraft configuration and the control system concurrently, trade-offs between these two design subspaces can improve the aircraft performance [28, 29].

For flexible aircraft, it is particularly advantageous to include the control system design as one of the disciplines and couple it with the aerodynamics and structures. This approach has the potential to exploit synergies between the three disciplines and yield higher performing aircraft than is possible without this multidisciplinary approach. Also, highly flexible aircraft can deform in unexpected ways under varying atmospheric conditions (e.g. Helios aircraft incident). Among the technical recommendations included in the investigation that followed the Helios crash, the development of more advanced multidisciplinary approaches that include control systems and time-domain analysis methods appropriate to flexible aircraft was emphasized [30].

The work presented in this paper integrates control system design in an aerostructural design optimization framework for flexible aircraft. Both time dependent maneuvers and gust excitations are considered in this optimization work. The main goal is to study the effect of the control system on the optimal design of the wing and its structure. The objective is to maximize the endurance by using an active control system and designing it concurrently with the aerodynamic shape and structural sizing. Parameters such as wing area, aspect ratio, taper ratio, and wing twist distribution were considered in the design optimization. Design constraints are enforced to ensure structural integrity, satisfactory stall behavior, and desirable flying qualities. The endurance is calculated based on cruise performance. The structural stresses are computed for the duration of an altitude gain maneuver and for the response due to a discrete $(1 - \cos)$ gust. The aeroservoelastic model involves the nonlinear equations of motion for a flexible aircraft based on the quasi-coordinate method, which has been derived in previous work by the authors [31, 32, 33]. A vortex-lattice panel method is used to evaluate the aerodynamic forces and moments, and the wing structure is modeled with a beam finite-element model.

In the remainder of this manuscript, the aeroservoelastic formulation is first presented and the general nonlinear form of the equations of motion for a deformable aircraft are derived. The equations for the aerostructural analysis and the state-space form of the linearized equations are then derived in Sections III and IV from the nonlinear equations. The optimization problem and the MDO framework are presented in Section V. Finally, the numerical results of different optimization cases and the conclusions are reported in Sections VI and VII, respectively.

II. Aeroservoelastic Formulation

As mentioned in the previous section, the quasi-coordinate method is adopted in this work to derive the aeroservoelastic equations of motion of a flexible aircraft. The quasi-coordinate method expresses the body movements with respect to a fixed reference frame. Fig. 1 shows a deformable aircraft with its original and deformed wing.

The inertial frame is denoted by $\mathbf{F}_I$, while $\mathbf{F}_B$ is used to denote the body-fixed frame, which is not necessarily connected to the center of mass. The absolute position and velocity of a infinitesimal mass element, $\mathrm{d}m$, on the aircraft is given by

$$\vec{R} = \vec{R}_c + \vec{r} + \vec{u} \tag{1}$$

$$\dot{\vec{R}} = \vec{V}_c + \vec{\omega} \times (\vec{r} + \vec{u}) + \dot{\vec{u}} \approx \vec{V}_c + \vec{\omega} \times \vec{r} + \dot{\vec{u}}. \tag{2}$$

The structural deformations can be expressed in a discrete finite-element formulation or it can be represented as a superposition of the aircraft structural vibration modes. Although the modal representation in dynamic response and stability analysis is widely used, aerostructural (static aeroelastic) analysis is usually based on finite-element methods

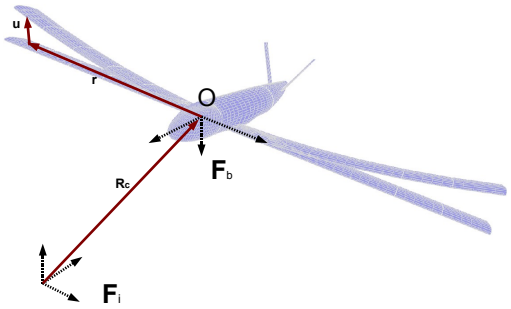

Figure 1. Deformed aircraft axis system

with thousands of degrees of freedom [34]. This is mainly due to the effect of concentrated forces, such as the weight of external stores, which the modal representation does not capture adequately, unless the structural modes are calculated using large fictitious masses at the locations of the lumped forces [35]. In this work, however, the following modal representation is used for both static and dynamic analysis:

$$\vec{u} = \sum_{i=1}^{n} \vec{\phi}_i \xi_i = \Phi \vec{\xi}, \tag{3}$$

where $\Phi = \left[\vec{\phi}_1, \ldots, \vec{\phi}_n\right]$ and $\vec{\xi} = \left[\xi_1, \ldots, \xi_n\right]^T$.

A. Kinetic Energy

The kinetic energy of a deformable aircraft can be formulated as follows:

$$\begin{aligned} T = \frac{1}{2}\int_v \rho \dot{\vec{R}}^T \dot{\vec{R}}\,\mathrm{d}v = \frac{1}{2} m \vec{V}_c^T \vec{V}_c + \vec{V}_c^T \left(\int_v \rho \tilde{r}^T\,\mathrm{d}v\right)\vec{\omega} + \\ + \vec{V}_c^T \underbrace{\left(\int_v \rho \Phi\,\mathrm{d}v\right)}_{S_1} \dot{\vec{\xi}} + \frac{1}{2}\vec{\omega}^T J \vec{\omega} + \vec{\omega}^T \underbrace{\left(\int_v \rho \tilde{r} \Phi\,\mathrm{d}v\right)}_{S_2} \dot{\vec{\xi}} + \frac{1}{2}\dot{\vec{\xi}}^T M_{ee} \dot{\vec{\xi}}, \end{aligned} \tag{4}$$

where J is the mass moment of inertia matrix for the rigid aircraft and $M_{ee} = \Phi^T M_{GG} \Phi$ is the modal elastic mass matrix. S_1 and S_2 are the rigid-elastic coupling terms that represent the interaction between the rigid and deformable dynamics. These terms are not the only source of coupling between the rigid and deformable dynamics; interaction also occurs through the aerodynamic forces and moments. If the origin of $\mathbf{F}_B$ is placed at the undeformed aircraft center of gravity, then $\int_v \rho \tilde{r}^T\,\mathrm{d}v = 0$ and the kinetic energy is,

$$T = \frac{1}{2} m \vec{V}_c^T \vec{V}_c + \vec{V}_c^T S_1 \dot{\vec{\xi}} + \frac{1}{2}\vec{\omega}^T J \vec{\omega} + \vec{\omega}^T S_2 \dot{\vec{\xi}} + \frac{1}{2}\dot{\vec{\xi}}^T M_{ee} \dot{\vec{\xi}}. \tag{5}$$

B. Potential Energy

The potential energy can be divided into two categories: gravitational energy and strain energy. The gravitational potential energy is,

$$U_g = -\int_v \rho \left(\vec{R}_c + \vec{r} + {C_{bi}}^T \vec{u}\right)^T \vec{g}\,\mathrm{d}v = -m \vec{R}_c^T \vec{g} - \vec{\xi}^T S_1^T C_{bi} \vec{g}. \tag{6}$$

The strain energy of an elastic system can be written as,

$$U = \frac{1}{2}\vec{\xi}^T K_{ee} \vec{\xi}, \tag{7}$$

where $K_{ee} = \Phi^T K_{GG} \Phi$ is the modal stiffness matrix.

C. Lagrange's Equation

The generalized coordinates in this problem are $\vec{R}_c$, $\vec{\theta}$, and $\vec{\xi}$. In aircraft flight dynamics, it is usually more convenient to express the translational and angular velocities in the body frame [36, 37], i.e.,

$$\vec{V}_c = C_{bi}\dot{\vec{R}}_c, \qquad \vec{\omega} = \underbrace{\begin{bmatrix} 1 & 0 & \sin\theta \\ 0 & \cos\phi & \cos\theta\sin\phi \\ 0 & -\sin\phi & \cos\theta\cos\phi \end{bmatrix}}_{D} \underbrace{\begin{Bmatrix} \dot{\phi} \\ \dot{\theta} \\ \dot{\psi} \end{Bmatrix}}_{\dot{\vec{\theta}}}. \tag{8}$$

However, the body frame velocities cannot be integrated. Therefore, the Lagrange equations in quasi-coordinates are used in this work [38, 39],

$$\frac{\mathrm{d}}{\mathrm{dt}}\left(\frac{\partial \mathfrak{L}}{\partial \vec{V}_c}\right) + \tilde{\omega}\frac{\partial \mathfrak{L}}{\partial \vec{V}_c} - C_{bi}\frac{\partial \mathfrak{L}}{\partial \vec{R}_c} = \vec{F} \tag{9}$$

$$\frac{\mathrm{d}}{\mathrm{dt}}\left(\frac{\partial \mathfrak{L}}{\partial \vec{\omega}}\right) + \tilde{V}_c\frac{\partial \mathfrak{L}}{\partial \vec{V}_c} + \tilde{\omega}\frac{\partial \mathfrak{L}}{\partial \vec{\omega}} - \left(D^T\right)^{-1}\frac{\partial \mathfrak{L}}{\partial \vec{\theta}} = \vec{M} \tag{10}$$

$$\frac{\mathrm{d}}{\mathrm{dt}}\left(\frac{\partial \mathfrak{L}}{\partial \dot{\vec{\xi}}}\right) - \frac{\partial \mathfrak{L}}{\partial \vec{\xi}} = \vec{f}_e, \tag{11}$$

where $\mathfrak{L} = T - V$. Substituting the kinetic and potential energy into Eqns. (9–11) and rearranging them, the equations of motion for the deformable aircraft become:

$$\begin{aligned} \begin{bmatrix} M & O_{3\times3} & S_1 \\ O_{3\times3} & J & S_2 \\ S_1^T & S_2^T & M_{ee} \end{bmatrix} \begin{Bmatrix} \dot{\vec{V}}_c \\ \dot{\vec{\omega}} \\ \ddot{\vec{\xi}} \end{Bmatrix} = &- \begin{bmatrix} m\tilde{\omega} & O_{3\times3} & \tilde{\omega}S_1 \\ O_{3\times3} & \tilde{\omega}J & \left(\tilde{V}_c S_1 + \tilde{\omega}S_2\right) \\ O_{n\times3} & O_{n\times3} & O_{n\times n} \end{bmatrix} \begin{Bmatrix} \vec{V}_c \\ \vec{\omega} \\ \dot{\vec{\xi}} \end{Bmatrix} \\ &- \begin{bmatrix} O_{6\times6} & O_{6\times n} \\ O_{n\times6} & K_{ee} \end{bmatrix} \begin{Bmatrix} \vec{R}_c \\ \vec{\theta} \\ \vec{\xi} \end{Bmatrix} + \begin{bmatrix} mC_{bi} \\ O_{3\times3} \\ S_1^T C_{bi} \end{bmatrix} \{\vec{g}\} + \begin{Bmatrix} \vec{F} \\ \vec{M} \\ \vec{f}_e \end{Bmatrix}, \end{aligned} \tag{12}$$

where, $\vec{F}$ and $\vec{M}$ are the total forces and moments in the body frame, including propulsive and aerodynamic forces. The generalized forces due to elastic deformations, $\vec{f}_e$, are calculated by integrating the product of the modes and nodal aerodynamic pressures over the surface, i.e.,

$$\vec{f}_e = \int_s \Phi^T \vec{P}\,\mathrm{d}s, \tag{13}$$

where, $\vec{P}$ represents the nodal aerodynamic pressure.

III. Aerostructural Analysis

The aerostructural model used in this work is shown in Fig. 2. Now that the equations of motion for a flexible aircraft have been derived, the steady-state equations can be obtained. In order to derive the equations for rectilinear flight, all derivatives are set to zero, and so is $\vec{\omega}$. The equations of motion for a flexible aircraft in a steady flight are,

$$\vec{F} + mC_{bi}\vec{g} = 0 \tag{14}$$

$$\vec{M} = 0 \tag{15}$$

$$-K_{ee}\vec{\xi} + (S_1)^T\vec{g} + \vec{f}_e = 0. \tag{16}$$

The above equations are coupled through the aerodynamic forces and moments, and can be used to find the trim parameters (α, δ_e), and the cruise condition wing deformation ($\vec{\xi}$). A Newton–Raphson method is used to solve the coupled system, with gradients computed using the complex-step derivative approximation [40]. In order to accelerate the algorithm, the gradient computations are parallelized and distributed over multiple cores.

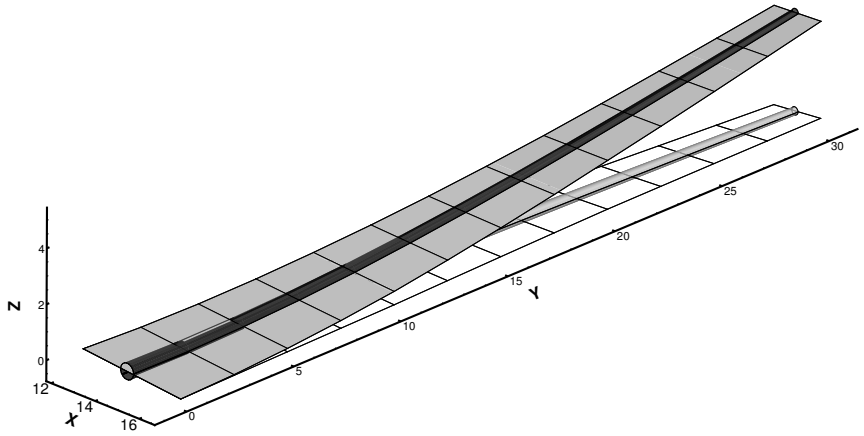

Figure 2. Aerostructural model

A. Structural Model

The aircraft fuselage and empennage are considered to be rigid. Grid finite elements — also known as torsional beams — are used to model the wing deformations. A grid element has two nodes, each with three degrees of freedom: displacement in the z direction and rotations about the x and y axes. The wing box is approximated as a hollow tube with variable wall thickness along the span. The stiffness and mass matrices for a grid element can be found in Paz and Leight [41]. The stress value is computed from the modal deflections using the following formulation:

$$\vec{\sigma} = SU\Phi\vec{\xi}, \tag{17}$$

where SU is a constant matrix that can be formed when the structural mesh is generated. During the course of the optimization, in order to maintain the same degree of accuracy as the wing structure is changed, the structure modes are re-constructed. Karpel suggests that in a minor design cycle, the structural mode shapes can be kept constant while the modal stiffness and mass matrices are being updated [35]. In this work, due to the application of a swarm-based optimizer, design variables can change significantly at each design cycle, preventing the use of sensitivity information to update stiffness and mass matrices. Therefore, the structural modes shapes are re-calculated for each design cycle evaluation and the stiffness and mass matrices are updated accordingly.

B. Aerodynamic Model

The vortex-lattice method (VLM) is used to calculate the aerodynamic forces and moments. Fig. 3 shows the vortex rings and wake vortices generated for the aerodynamic analysis of the aircraft. The panel and wake vorticities are calculated by enforcing the tangential flow condition at each panel and enforcing the Kutta condition at the trailing edge. The calculated vorticity at each panel is then used to calculate the pressure on each panel; then the rigid and elastic aerodynamic forces and moments can be calculated as follows:

$$\vec{F}_{\text{aero}} = \sum_{j=1}^{n_s}\sum_{k=1}^{n_c} p_{jk}\hat{n}_{jk}\Delta A_{jk} \tag{18}$$

$$\vec{M}_{\text{aero}} = \sum_{j=1}^{n_s}\sum_{k=1}^{n_c} \tilde{r}\left(p_{jk}\hat{n}_{jk}\right)\Delta A_{jk} \tag{19}$$

$$\vec{f}_{e_i} = \sum_{j=1}^{n_s}\sum_{k=1}^{n_c} \phi_i|_{jk}\,.p_{jk}\hat{n}_{jk}\Delta A_{jk}, \tag{20}$$

where p_{jk}, A_{jk}, and $\hat{n}_{jk}$ are the pressure, area, and normal vector for panel j,k, respectively, and $\phi_i|_{jk}$ is the deflection due to structural mode i at panel j,k. The summation ranges, n_c and n_s, show the number of elements along the chordwise and spanwise directions, respectively.

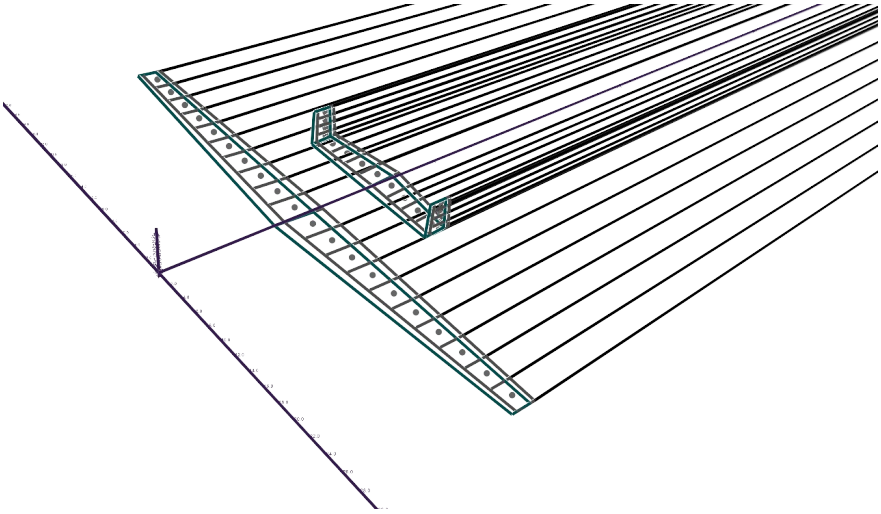

Figure 3. Sample vortex lattice model

In order to capture the unsteady aerodynamic loads, a wake roll-up routine has to be linked with the current vortex-lattice method. Although such unsteady aerodynamic code can be used directly to calculate the unsteady loads to perform a time-domain gust analysis, the computational burden of this method has made it less attractive to aeroservoelastic practitioners. In order to overcome the above challenge, reduced-order models (ROMs) based on the Volterra theory of nonlinear systems have gained significant attention. The Volterra theory was first used to model unsteady aerodynamic systems by Silva [42] and has since been developed further by other researchers [43, 44, 45, 46]. The combination of this method with a system identification technique such as eigensystem realization algorithm (ERA) can be used to construct state-space matrices (A,B, and C) that represent the generalized aerodynamic forces. More detailed information on the application of the Volterra theory and the ERA to the unsteady aerodynamic modeling can be found in the literature [46]. In this work, however, the dynamic gust response analysis is performed using the quasi-steady aerodynamic loads. The use of quasi-steady aerodynamic loads can help reduce the computational burden.

IV. Aeroservoelastic Control

Substituting the perturbed flight parameters into Eq. (12) and using the first order approximation, the linearized equations about a steady-state rectilinear flight condition become,

$$\begin{Bmatrix} \delta\dot{\vec{V}}_c \\ \delta\dot{\vec{\omega}} \\ \ddot{\vec{\xi}} \end{Bmatrix} = M^{-1} \begin{bmatrix} m\tilde{V}_{c,0}\delta\vec{\omega} - m\left(\delta C\right)\vec{g} + \delta\vec{F} \\ -\tilde{V}_{c,0}S_1\dot{\vec{\xi}} + \delta\vec{M} \\ K_{ee}\delta\vec{\xi} + \delta\vec{f}_e \end{bmatrix}. \tag{21}$$

Performing sensitivity analysis on aerodynamic forces and moments and substituting into Eq. (21), the state-space representation of an aeroservoelastic aircraft can be written as

$$\vec{x} = \left\{ \vec{V} \quad \vec{\omega} \quad \vec{\xi} \quad \dot{\vec{\xi}} \quad \vec{\theta} \quad h \right\}^T \tag{22}$$

$$\dot{\vec{x}} = A\vec{x} + B\vec{u} + B_w w_g \tag{23}$$

$$\vec{y} = C\vec{x} \tag{24}$$

$$\vec{z} = E\vec{x} \tag{25}$$

where $\vec{\theta}$ is a vector of Euler angles, $\left\{ \phi \quad \theta \quad \psi \right\}^T$. The effect of a gust on the aircraft is modeled by the matrix B_w. The state-space matrices for an aeroservoelastic aircraft are presented in Appendix A. Elevator and aileron deflections are the two control inputs used in this work. The left and the right ailerons deflect differentially for roll control and can

also deflect individually to perform load alleviation. The total control surface deflection for each aileron is calculated by adding these two deflections.

By analyzing the system matrices, it can be shown that the current configuration is controllable. In order to make this system observable, the wing deflection has to be measured at least at two points. In this representation, $\vec{y}$ is the tracked output, which is the aircraft altitude, while $\vec{z} = \begin{Bmatrix} h & \delta_{\text{tip}} & \delta_{\text{mid}} \end{Bmatrix}^T$ is the measured output, which includes the altitude and wing vertical deflections at the tip and mid-span. Based on the measured parameters, an observer is designed to provide all states to the controller.

The structural stresses in the wing are directly proportional to the modal displacements, as shown in Eq. (17). Therefore, by regulating them to zero, the instantaneous stress can be controlled to be closer to the cruise level.

Based on the above explanation, the state-space representation is used to design a control system that performs altitude tracking and regulates structural deformations in order to lower the maximum stress during the maneuver. We use a linear quadratic (LQ) controller, with the cost function

$$J = \int \left(\vec{x}^T Q \vec{x} + \vec{u}^T R \vec{u} \right) \, \mathrm{d}t. \tag{26}$$

The key for designing a successful LQ controller is the selection of the weighting matrices Q and R. We assemble the Q matrix using two coefficients: q_{rigid} and q_{elastic}, yielding

$$Q = \text{diag} \left(\underbrace{q_{\text{rigid}}, \ldots, q_{\text{rigid}},}_{6} \quad \underbrace{q_{\text{elastic}}, \ldots, q_{\text{elastic}},}_{2n} \quad q_{\text{rigid}}, \quad \cdots \right). \tag{27}$$

These two variables are assigned to the optimizer as design variables. In order to speed up the optimization process, the R matrix that is used to penalize the control deflections is fixed during the optimization. A proper value for the R matrix is selected by trial and error before starting the optimization.

The control input to the system is $\vec{u} = -K(\vec{x} - \vec{x}_{\text{ref}})$, where K is the gain matrix, and $\vec{x}_{\text{ref}}$ represents the desired values for the state vector. In order to design a realistic control system, control surface deflections are limited by upper and lower bounds. Two cases are presented below to highlight the effect of the proposed control system on the aircraft structural loading; the obtained results are presented in Section VI.

V. Problem Formulation

A. Design Variables

The objective of this framework is to surpass the current aircraft endurance limits through the use of an active load alleviation system that is designed concurrently with the rest of the aircraft. In the optimization problem solved here, design variables from all three disciplines are included. The aerodynamic design variables are the aspect ratio (AR), wing area, and the wing spanwise twist distribution (γ_i). The structural sizing is represented by the spar wall thicknesses (t_i). Finally, the weighting parameters q_{rigid} and q_{elastic}, are the control discipline design variables.

B. Flight Conditions

Two different flight conditions are analyzed here: an altitude change maneuver and a flight through a sharp vertical gust. Both conditions are selected to study the effect of inertial and aerodynamic loads on aircraft structure and the design optimization. It should be noted that both study cases represent longitudinal flight conditions. In the first maneuver, the aircraft is commanded to gain 1,000m in 40s. Unfortunately, there are no published performance requirements for high-altitude long-endurance very flexible aircraft. However, Shearer and Cesnik [47] have considered a very flexible aircraft as a large transport type aircraft (class III-L) and used a maximum climb rate of 10.16m/s at sea level as a guideline for control design. In this work, a fast maneuver is performed resulting in large wing loadings. For the second flight condition, a $(1 - \cos)$ discrete gust profile is used to generate large wing loadings. The gust profile is generated using

$$w_g = \frac{\bar{w}_g}{2} \left(1 - \cos \frac{2\pi t}{L_g} \right), \tag{28}$$

where $\bar{w}_g$ is the maximum gust velocity, and L_g is the gust length, in terms of the time needed for a point in the aircraft to travel across its length. In this work $\bar{w}_g$ is set to 4.575m/s and a value of 0.5s is used for gust length.

C. Constraints

Two constraints are enforced: one guarantees the structural integrity by constraining the maximum stress in the structure for the duration of the maneuver or gust; while the other ensures maneuvering capability by limiting the altitude error at 40s after the start of the maneuver. The aircraft is required to climb from 2,000m to 3,000m. The addition of the altitude constraint at 40s ensures that the optimizer achieves load alleviation capability without sacrificing the aircraft maneuverability. A gust strength of 4.575m/s (15 fps) is used for the optimization, which is the same as the gust strength used for the control system simulation.

In order to reduce the number of structural constraints, the constraints are aggregated using the Kreisselmeier–Steinhauser (KS) function [48]. For a vector of constraints $g_i \leq 0 \quad (i = 1, \ldots, n)$ the KS function is a differentiable function that has the form,

$$KS\left(g_i\right) = \frac{1}{\rho_{KS}} \ln \sum_{i=1}^{n} e^{\rho_{KS} g_i}, \tag{29}$$

where ρ_{KS} is a parameter that controls the proximity of the function to the maximum of the constraints, as we can infer from the inequality property,

$$g_{\max} \leq KS(g_i) \leq g_{\max} + \frac{\ln(n)}{\rho_{KS}}. \tag{30}$$

Based on this property, all stress constraints can be enforced by the single constraint,

$$KS\left(g\left(\sigma_i\right)\right) < 0, \tag{31}$$

where,

$$g_i\left(\sigma_i\right) = \frac{\sigma_i}{\sigma_{\text{yield}}} - 1. \tag{32}$$

A more detailed analysis of the properties of KS function and its application to optimization problems can be found in previous work [48, 49].

In this optimization, the taper ratio is fixed. Therefore, increasing the aspect ratio may decrease the wing chord, resulting in high sectional lift coefficients near the wing tips. In order to avoid tip stall, the stall speed of the designed wing is required to be smaller than that of the baseline wing. In order to satisfy this condition, all sectional lift coefficients must be lower than $C_{l_{\max}}$, the maximum sectional lift coefficient of the baseline wing, *i.e.*

$$V_s \leq V_{s_{\text{ref}}} \Rightarrow C_{l_i}|_{V_{s_{\text{ref}}}} \leq C_{l_{\max}} \tag{33}$$

The same technique used for aggregating the structural constraints is used to aggregate the the stall constraints:

$$KS\left(g\left(C_{l_i}\right)\right) \leq 0, \tag{34}$$

where,

$$g\left(C_{l_i}\right) = \frac{C_{l_i}}{C_{l_{\max}}} - 1. \tag{35}$$

In this design problem, the thickness-to-chord ratio is fixed for the whole wing, and therefore, the spar diameter depends on the local chord. Ultimately, this means that the spar diameter decreases as the aspect ratio increases. The spar wall thickness is bounded below by the minimum gauge thickness and above by the spar radius. Spar thicknesses and wing twist angles are varied at six locations along the span, and the intermediate values are linearly interpolated.

D. Optimization Problem

The complete optimization problem is as follows:

$$\min_{AR,S_{\text{ref}},t_i,\gamma_i,q_{\text{rigid}},q_{\text{elastic}}} \; -\frac{C_L}{C_D}\ln\frac{W_{\text{initial}}}{W_{\text{empty}}}$$

$$\text{subject to} \begin{cases} KS\left(g\left(\sigma_i\right)\right) \leq 0 \\ KS\left(g\left(C_{l_i}\right)\right) \leq 0 \\ h_{\text{err}} \leq 0.05 \\ t_i - \dfrac{d_i}{2} \leq 0 \qquad \text{where } (i = 1, \ldots, n). \\ -10 \leq \gamma_i \leq 10 \\ 145 \leq S_{\text{ref}} \leq 245 \\ 10 \leq AR \leq 20 \\ 10 \leq q_{\text{rigid}} \leq 100 \\ 500 \leq q_{\text{elastic}} \leq 1500 \end{cases} \tag{36}$$

Since the wing area (S_{ref}) can change during the course of the optimization, the viscous drag must be considered in the endurance calculation. The drag coefficient used in this work takes into account both the induced drag and the viscous drag. The induced drag is calculated using the previously described vortex-lattice panel code; the viscous drag is estimated using an empirical formulation based on the wet-surface area.

While the structural and aerodynamic parameters directly affect the endurance through weight and aerodynamic performance, the control parameters have an indirect effect on the objective function through load alleviation. A simple linear control theory can be used to explain the effect of the control parameters on the final design. A system's steady-state error is dependent on the choice of gain matrix, K. Therefore, different values of control weighting parameters result in different gain matrices that can affect the altitude constraint. However, maximum stress can be related to the maximum overshoot of the structural modes amplitudes, which is related to the eigenvalues of the system. The system's eigenvalues depend on the gain matrix, which itself depends on the weighting parameters. The limits for q_{rigid} and q_{flexible} are selected through a trial-error process. Although the R matrix is selected to penalize the control deflections and avoid controls saturation, large values of q_{rigid} and q_{flexible} can result in controls saturation over a long period of time, which can destabilize the aircraft. Therefore, an upper limit is used to avoid prolonged controls saturation. However, as this type of aircraft is marginally stable, a sharp atmospheric gust can result in excessive oscillations. As a result, a lower bound is set in place for q_{rigid} and q_{flexible} to avoid low gain controllers that cannot damp out the gust-induced oscillations effectively. The flow diagram for the aeroservoelastic optimization is shown in Fig. 4.

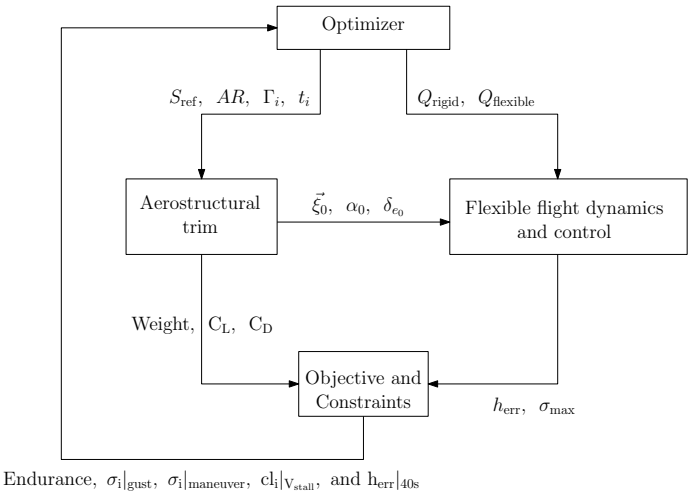

Figure 4. Aeroservoelastic optimization flow diagram

An augmented Lagrange multiplier particle swarm optimizer (ALPSO) is used to solve the proposed optimization

problem. This is a gradient-free algorithm that tends to find global optima, and this particular version can solve constrained problems [50]. Due the presence of multiple local minima, a gradient-free optimizer is chosen over a gradient-based optimizer.

VI. Results

A. Baseline Model

A high altitude long endurance (HALE) UAV with a large aspect ratio is the focus of this study. The geometry of the baseline aircraft is shown in Fig. 5 and the geometric parameters are listed in Table 1. More detailed information about this UAV can be found in Shearer and Cesnik [23, 47].

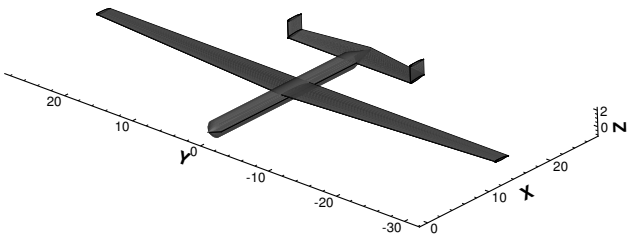

Figure 5. 3D geometry of a generic high aspect ratio UAV

Table 1. Aircraft geometric properties

Property	Value
Fuselage length	26.4 m
Wing span	58.6 m
Wing area	196 m^2
Wing taper	0.48
Horizontal tail span	18 m
Horizontal tail area	53.5 m^2
Horizontal tail taper	0.7
Vertical tail span	4 m
Vertical tail area	8.9 m^2
Vertical tail taper	0.81

The chord-wise location of the spar is set to 45% of the chord. The design cruise and stall speeds are set to 80m/s and 60m/s, respectively. A maximum airfoil lift coefficient of 1.6 is used for the stall calculations. The value of ρ_{KS} in the KS function is set to 100. The initial and final altitudes for the altitude gain maneuver are set to 2,000m and 3,000m, respectively.

B. Control System Design

The proposed control system is integrated with the aircraft dynamics. First, a control system that performs an altitude gain maneuver with and without load alleviation is designed. The results highlight the effect of the load alleviation system on the maximum stress ($\sigma_{\max}$) value. As shown in Fig. 6, both control systems show satisfactory climb performance. However, when the load alleviation system is used, the same climb rate can be achieved with lower structural stresses, as seen in Fig. 6 . This is due to the fact that when load alleviation is used, the structural relaxation is performed by applying the ailerons, as shown in Fig. 7. As expected, lower elevator deflections are applied when the load alleviation is not used. When the load alleviation is used, the structural stresses induced by a faster maneuver (higher elevator deflection) are suppressed by applying the ailerons symmetrically.

Another simulation was performed to show the gust load alleviation capability of the control system. The results are shown in Figs. 8 and 9. The load alleviation system reduces the structural stress significantly. However, when the system is off, the controller cannot stabilize the aircraft within the same time period. The absence of the load alleviation system causes excessive structural stress when the aircraft is passing through atmospheric turbulence.

C. Aeroservoelastic Optimization

Two design optimization cases are considered: one with load alleviation and the other without. The optimized endurance and design variable values are summarized in Table 2 and Figs. 10 and 11. The constraint results are shown in Figs. 12 and 13, where the horizontal lines represent the stall and the stress constraint values, respectively.

The optimization results presented in Table 2 show that the optimization of the load alleviation system in the design procedure results in a significantly lighter wing structure (41.5% lighter). The optimization results plotted in Fig. 10 show that the spar thickness decreases monotonically when load alleviation is used. However, the optimal thickness distribution is different when load alleviation is not employed: a significant amount of material is added

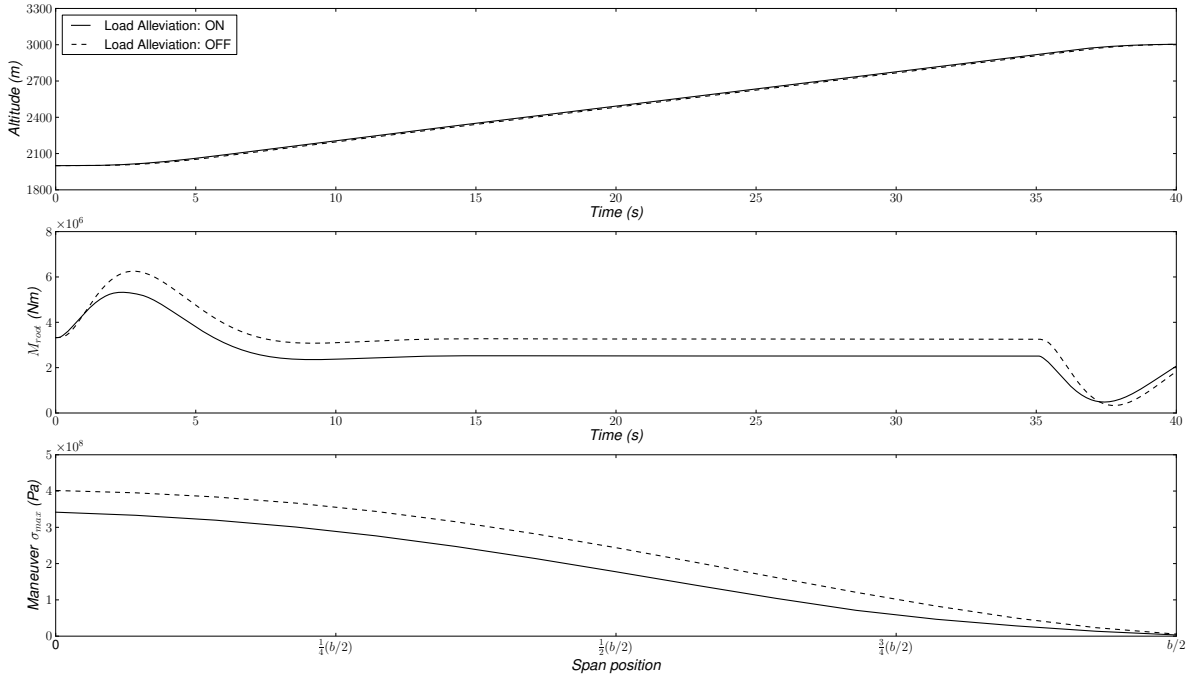

Figure 6. Altitude and bending moment time history for climb maneuver

Table 2. Optimization results with and without load alleviation system.

Load alleviation	Off	On
S_{ref} (m^2)	219.18	191.47
AR	13.98	14.03
L/D	34.29	34.37
q_{elastic}	1499.95	1499.88
q_{rigid}	90.63	75.71
Wing mass (kg)	13,378	7,817
Endurance factor	31.90	38.83

near the tip. When the active load alleviation system is not used, the optimizer is forced to explore passive design options. Increasing the wing tip mass can help stabilize the aircraft and lower the maximum stress when encountering an atmospheric turbulence. The increase of the wing tip thickness effectively adds mass to the wing tip.

It can be shown that a lower added tip mass would result in control effector saturation and aircraft instability. In this work, only an upward wind gust is considered. However, increasing the wing tip mass would also be helpful in reducing the maximum stress of a flexible wing passing through a downward gust. In order to satisfy the stress constraints without using the added mass at the tip, a much higher thickness near the wing root would be required, resulting in a far heavier aircraft.

The converged values of control weighting parameters listed in Table 2 and the altitude and load factor time history (Fig. 13) show that both the cases achieve comparable performance in the climb maneuver.

Fig. 12 shows the lift coefficient distribution at the reference stall speed of 60m/s. The stall constraint is satisfied in both cases. However, when load alleviation is not employed, the wing area is 14.5% higher than the wing area when load alleviation is considered. This is mainly due to the weight of the wing structure, which is 41.5% higher than the weight of the wing that uses the load alleviation system.

Finally, the results show that the aircraft endurance is increased by 21.7% when an active load alleviation system is used and optimized concurrently with the wing aerodynamics and structural sizing.

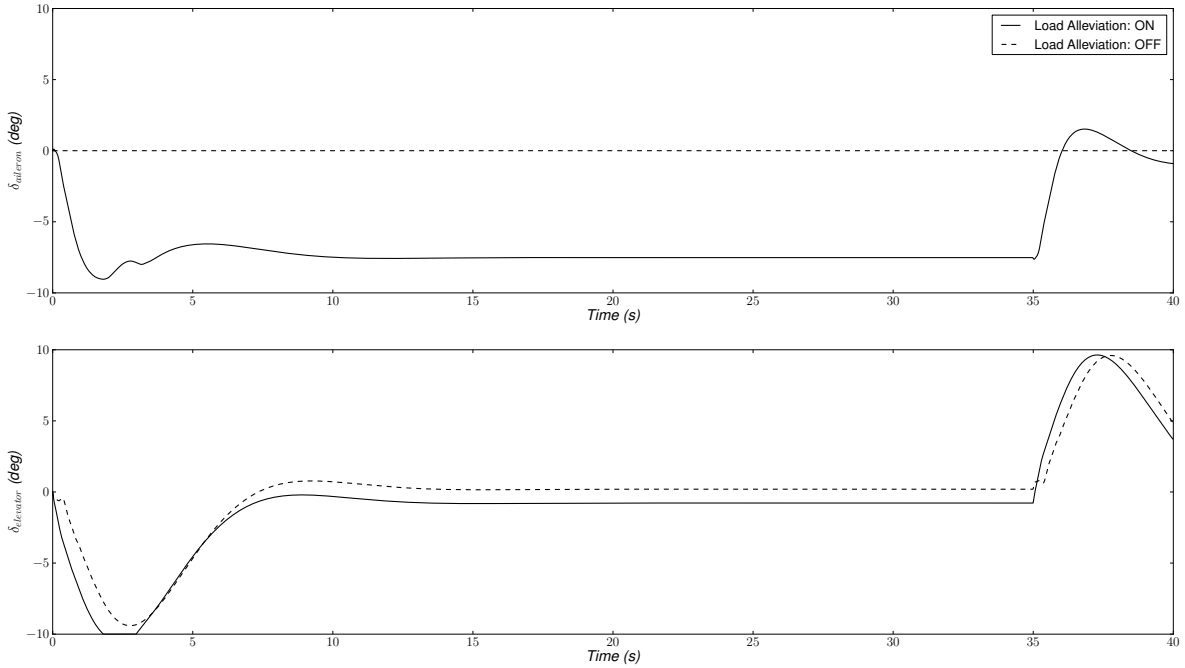

Figure 7. Control effectors deflection time history for climb maneuver

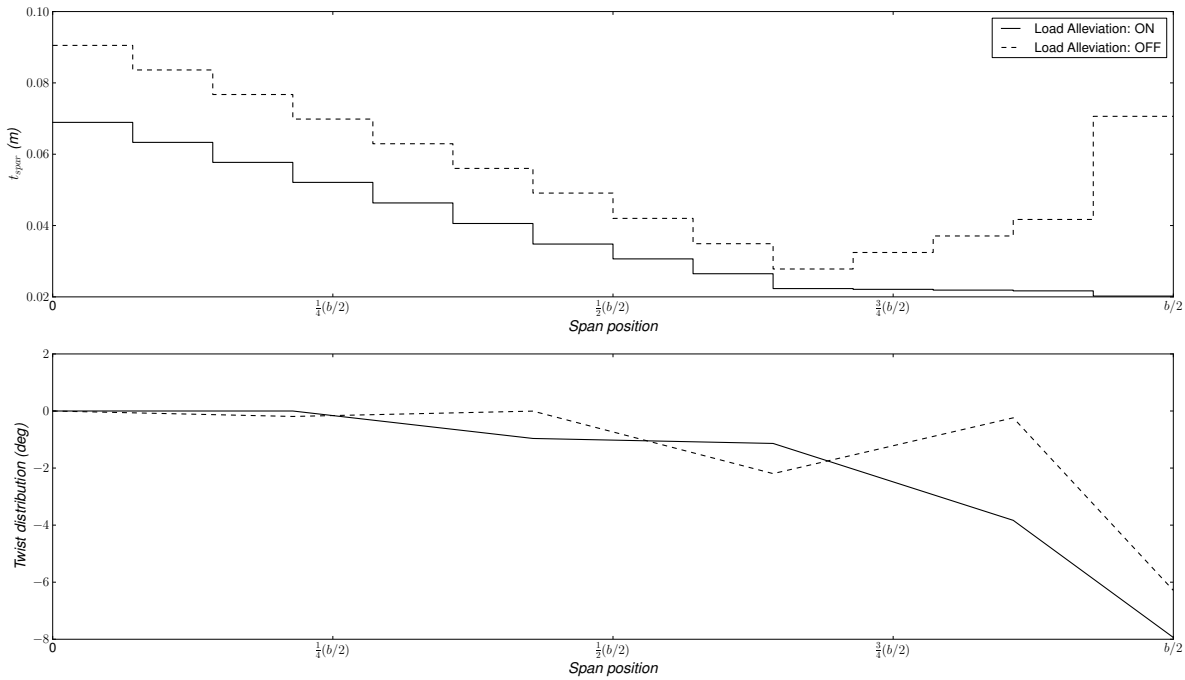

Figure 10. Spanwise distribution of spar wall thickness and wing twist

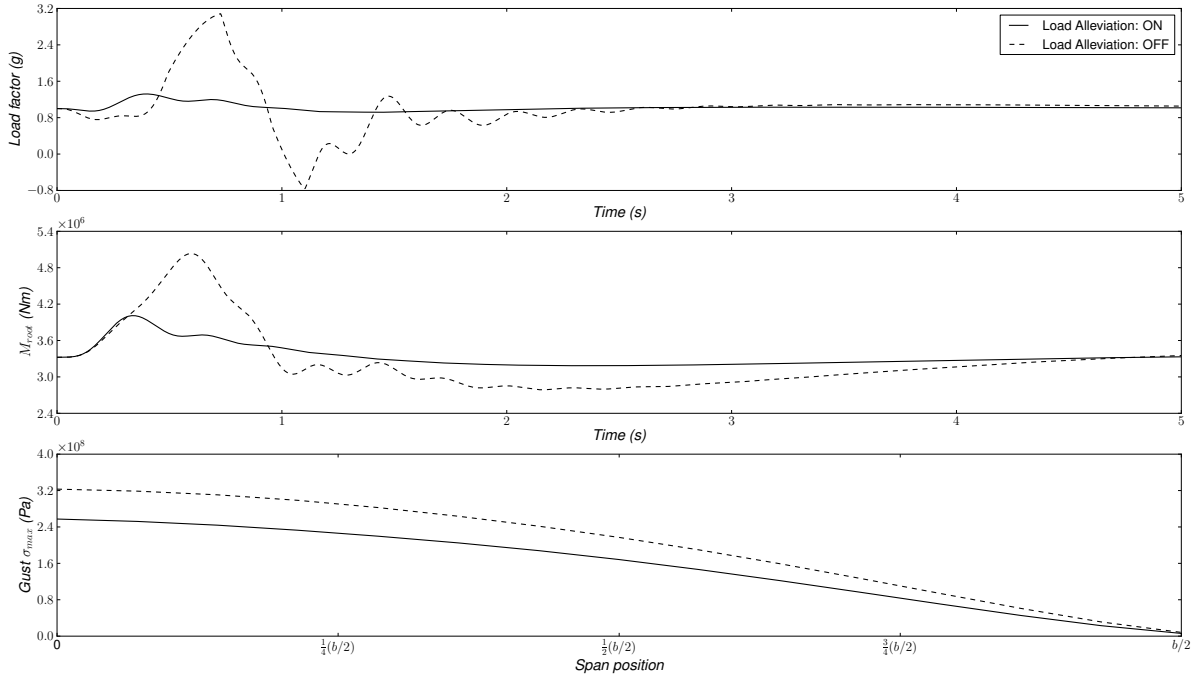

Figure 8. Load factor, bending moment and maximum stress time history due to gust excitation

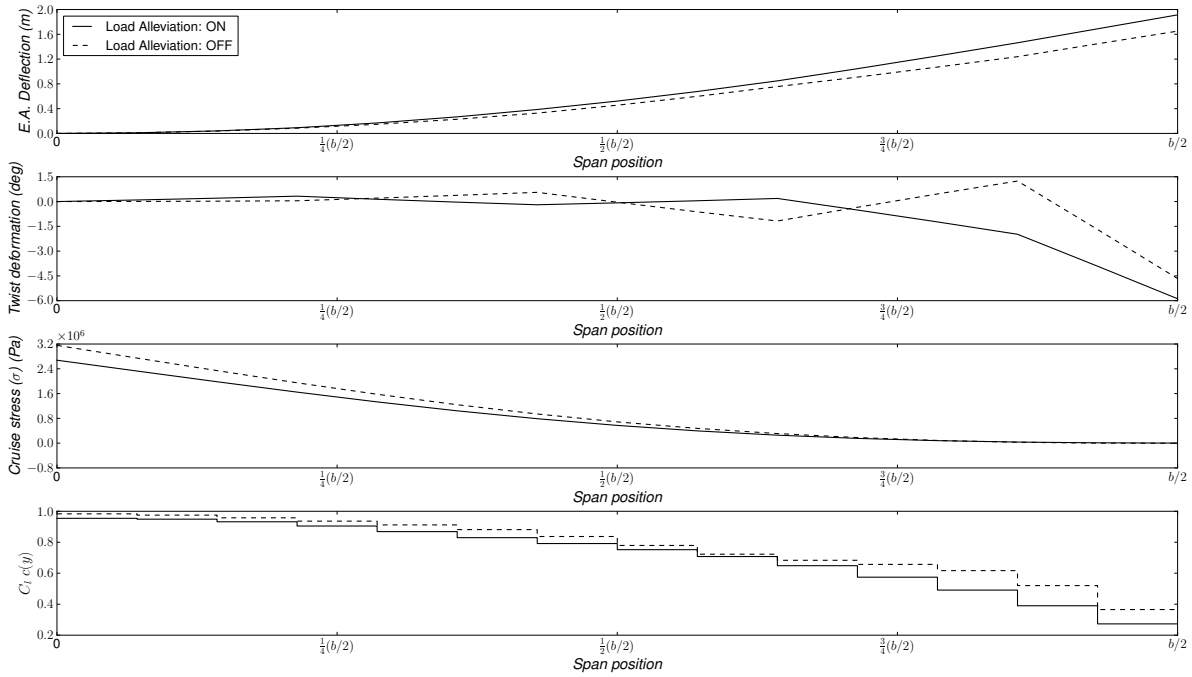

Figure 11. Spanwise distribution of vertical displacement, stress, and lift at the cruise condition

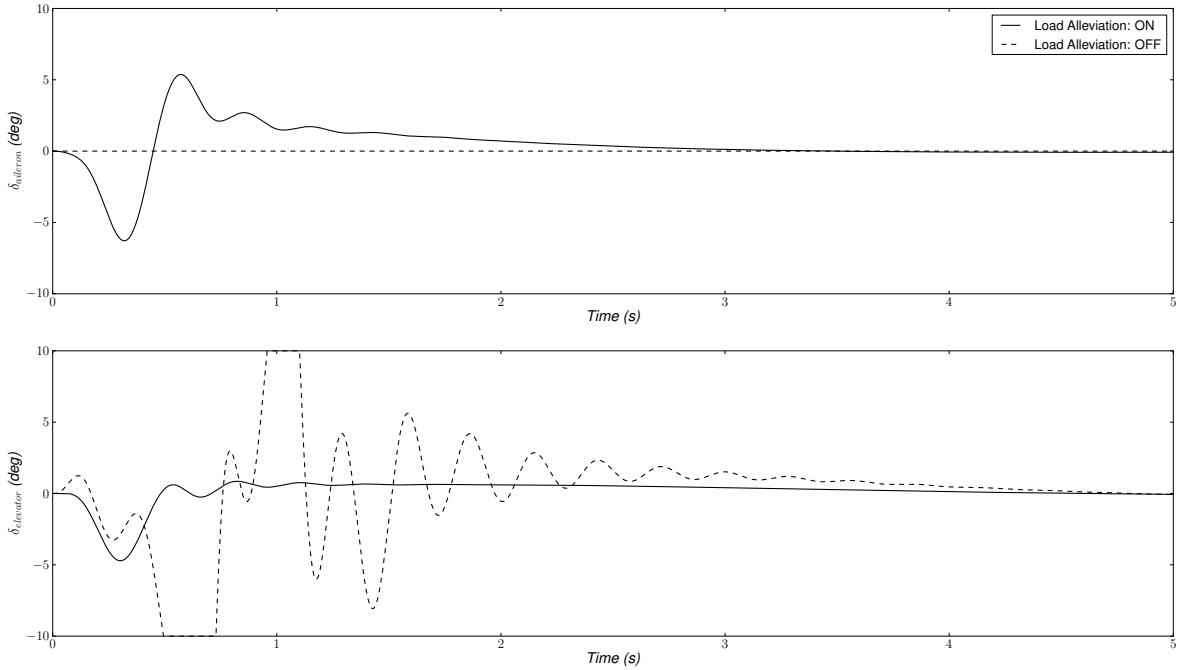

Figure 9. Control effectors deflection time history in response to gust excitation

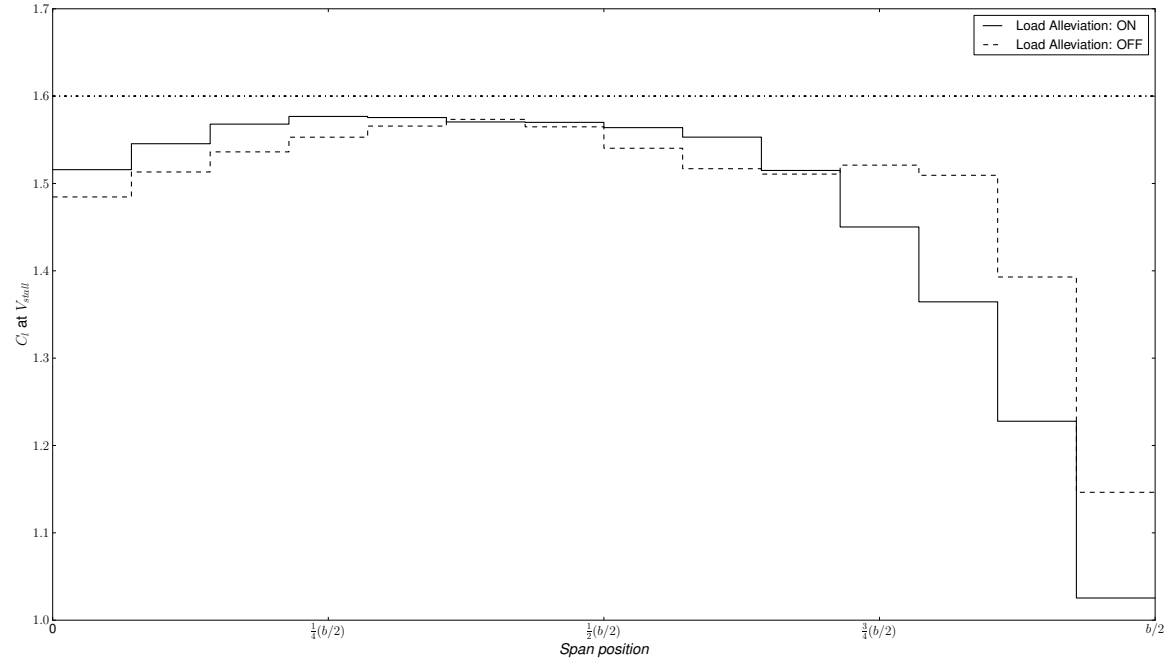

Figure 12. Spanwise C_l distribution at the minimum allowable speed

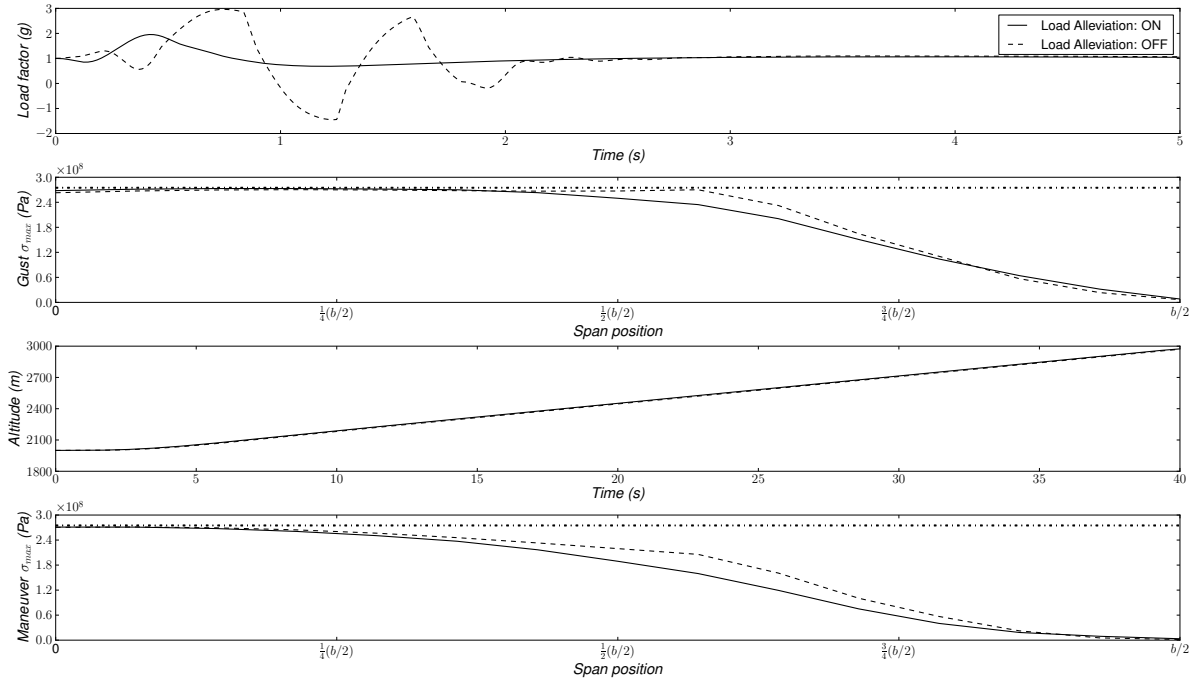

Figure 13. Load factor, altitude and maximum stress time history (stress and maneuver constraints)

VII. Conclusions

In this work, the design optimization of an active load alleviation control system has been integrated with the the design optimization of the aerodynamic shape and structural sizing of a UAV. The equations of motion for an aircraft with a flexible wing were derived in order to perform the time-dependent analysis, which can handle large rigid-body motions with structural deformations. The analysis framework was used to compare two design cases: one for which the control system simply worked towards achieving or maintaining a target altitude, and another where the control system was also performing load alleviation. The use of the active load alleviation system resulted in a 21.7% improvement in the endurance relative to the optimum result without load alleviation. The results show that the inclusion of control system discipline along with other disciplines at the early stages of aircraft design improves aircraft performance. It was also shown that structural stresses due to gust excitations can be better controlled by the use of active structural control systems. In the future, we expect that the inclusion of more sophisticated maneuvers, including asymmetric ones, will show that the integration of the active load alleviation system design with the design of the wing will result in further increases in performance.

Appendix

Appendix A

The state-space matrices for an aeroservoelastic aircraft are presented here. The A matrix represents the system dynamics and the B and C matrices are the control and output matrices, respectively. These matrices represent both longitudinal and lateral-directional dynamics of a flexible aircraft.

$$A = \begin{bmatrix} M^{-1}\frac{\partial \vec{F}}{\partial \vec{V}} & M^{-1}\frac{\partial \vec{F}}{\partial \vec{\omega}} + \tilde{V}_0 & M^{-1}\frac{\partial \vec{F}}{\partial \vec{\xi}} & M^{-1}\frac{\partial \vec{F}}{\partial \dot{\xi}} & \begin{bmatrix} 0 & -C\theta_0 \cdot g \\ C\theta_0 \cdot g & 0 \\ 0 & S\theta_0 \cdot g \end{bmatrix} \\ J^{-1}\frac{\partial \vec{M}}{\partial \vec{V}} & J^{-1}\frac{\partial \vec{M}}{\partial \vec{\omega}} & J^{-1}\frac{\partial \vec{M}}{\partial \vec{\xi}} & J^{-1}\frac{\partial \vec{M}}{\partial \dot{\xi}} - J^{-1}\tilde{V}_0 S_1 & O_{3\times 2} \\ O_{n\times 3} & O_{n\times 3} & O_{n\times n} & I_{n\times n} & O_{n\times 2} \\ M_{ee}^{-1}\frac{\partial \vec{f}_e}{\partial \vec{V}} & M_{ee}^{-1}\frac{\partial \vec{f}_e}{\partial \vec{\omega}} & M_{ee}^{-1}\left(\frac{\partial \vec{f}_e}{\partial \vec{\xi}} - K_{ee}\right) & M_{ee}^{-1}\frac{\partial \vec{f}_e}{\partial \dot{\xi}} & O_{n\times 2} \\ O_{2\times 3} & I_{2\times 3} & O_{2\times n} & O_{2\times n} & O_{2\times 2} \end{bmatrix}$$

$$B = \begin{bmatrix} M^{-1}\frac{\partial \vec{F}}{\partial \delta_a} & M^{-1}\frac{\partial \vec{F}}{\partial \delta_e} \\ J^{-1}\frac{\partial \vec{M}}{\partial \delta_a} & J^{-1}\frac{\partial \vec{M}}{\partial \delta_e} \\ O_{n\times 1} & O_{n\times 1} \\ M_{ee}^{-1}\frac{\partial \vec{f}_e}{\partial \delta_a} & M_{ee}^{-1}\frac{\partial \vec{f}_e}{\partial \delta_e} \\ O_{2\times 1} & O_{2\times 1} \end{bmatrix}$$

$$B_w = \begin{bmatrix} M^{-1}\frac{\partial \vec{F}}{\partial \vec{V}} & M^{-1}\frac{\partial \vec{F}}{\partial \vec{\omega}} \\ J^{-1}\frac{\partial \vec{M}}{\partial \vec{V}} & J^{-1}\frac{\partial \vec{M}}{\partial \vec{\omega}} \\ O_{n\times 3} & O_{n\times 3} \\ M_{ee}^{-1}\frac{\partial \vec{f}_e}{\partial \vec{V}} & M_{ee}^{-1}\frac{\partial \vec{f}_e}{\partial \vec{\omega}} \\ O_{2\times 3} & O_{2\times 3} \end{bmatrix}$$

Acknowledgments

The authors would like to thank the Natural Sciences and Engineering Research Council of Canada (NSERC) for providing financial support for this project.

References

[1] Guinta, A. A., Golividov, O., Knill, D. L., Grossman, G., Haftka, R. T., Mason, W. H., and Watson, L. T., "Multidisciplinary Design Optimization of Advanced Aircraft," *15th International Conference on Numerical Methods in Fluid Dynamics*, Lecture Notes in Physics, 1996, pp. 14–34.

[2] Sobieski, J. and Haftka, R., "Multidisciplinary Aerospace Design Optimization: Survey of Recent Developments," *Structural Optimization*, Vol. 14, No. 1, 1997, pp. 1–23.

[3] Martins, J. R. R. A., Alonso, J. J., and Reuther, J. J., "High-Fidelity Aerostructural Design Optimization of a Supersonic Business Jet," *Journal of Aircraft*, Vol. 41, No. 3, 2004, pp. 523–530.

[4] Ning, S. A. and Kroo, I. M., "Multidisciplinary Considerations in the Design of Wings and Wing Tip Devices," *Journal of Aircraft*, Vol. 47, No. 2, 2010, pp. 534–543.

[5] Jansen, P., Perez, R. E., and Martins, J. R. R. A., "Aerostructural Optimization of Nonplanar Lifting Surfaces," *Journal of Aircraft*, Vol. 47, No. 5, 2010, pp. 1491–1503.

[6] Woods-Vedeler, J. and Pototzky, A., "Rolling Maneuver Load Alleviation Using Active Controls," *Journal of Aircraft*, Vol. 32, No. 1, 1995, pp. 68–76.

[7] Suzuki, S., "Simultaneous Structure/Control Design Synthesis for Aero-Servo-Elastic System," *Finite Elements in Analysis and Design*, Vol. 14, No. 2–3, October 1993, pp. 197–208.

[8] Nam, C., Chattopadhyay, A., and Kim, Y., "Optimal Wing Planform Design for Aeroelastic Control," *AIAA Journal*, Vol. 38, No. 8, 2000, pp. 1455–1470.

[9] Moulin, B. and Karpel, M., "Gust Loads Alleviation Using Special Control Surfaces," *Journal of Aircraft*, Vol. 44, No. 1, 2007, pp. 17–25.

[10] Gaulocher, S., Roos, C., and Cumer, C., "Aircraft Load Alleviation During Maneuvers Using Optimal Control Surface Combinations," *Journal of Guidance, Control, and Dynamics*, Vol. 30, No. 2, 2007, pp. 591–600.

[11] Livne, E., "Integrated Aeroelastic Optimization: Status and Direction," *Journal of Aircraft*, Vol. 36, No. 1, 1999, pp. 122–145.

[12] Livne, E., "Future of Airplane Aeroelasticity," *Journal of Aircraft*, Vol. 40, 2003, pp. 1066–1092.

[13] Idan, M., Karpel, M., and Moulin, B., "Aeroservoelastic Interaction Between Aircraft Structural and Control Design Schemes," *Journal of Guidance, Control, and Dynamics*, Vol. 22, No. 4, 1999, pp. 513–519.

[14] Moulin, B., Idan, M., and Karpel, M., "Aeroservoelastic Structural and Control Optimization Using Robust Design Schemes," *Journal of Guidance,Control, and Dynamics*, Vol. 25, No. 1, 2002, pp. 152–159.

[15] Zink, S., Raveh, D., and Mavris, D., "Integrated Trim and Structural Design Process for Active Aeroelastic Wing Technology," *Journal of Aircraft*, Vol. 40, No. 3, 2003, pp. 523–531.

[16] Zink, S., Raveh, D., and Mavris, D., "Robust Structural Design of an Active Aeroelastic Wing with Maneuver Load Inaccuracies," *Journal of Aircraft*, Vol. 41, No. 3, 2004, pp. 585–593.

[17] Pendleton, E., Bessette, D., Field, P., Miller, G., and Griffin, K., "Active Aeroelastic Wing Flight Research Program: Technical Program and Model Analytical Development," *Journal of Aircraft*, Vol. 37, No. 4, 2000, pp. 554–561.

[18] Rodden, W. P. and Love, J. R., "Equations of Motion of a Quasisteady Flight Vehicle Utilizing Restrained Static Aeroelastic Characteristics," *Journal of Aircraft*, Vol. 22, No. 9, 1985, pp. 802–809.

[19] Waszak, M. R. and Schmidt, D. K., "Flight Dynamics of Aeroelastic Vehicles," *Journal of Aircraft*, Vol. 25, No. 6, 1988, pp. 563–571.

[20] Schmidt, D. K. and Raney, D. L., "Modeling and Simulation of Flexible Flight Vehicles," *Journal of Guidance, Control and Navigation*, Vol. 24, No. 3, 2001, pp. 539–546.

[21] Meirovitch, L. and Tuzcu, I., "Integrated Approach to the Dynamics and Control of Maneuvering Flexible Aircraft," Tech. Rep. CR-2003-211748, NASA, June 2003.

[22] Patil, M. J. and Hodges, D. H., "Flight Dynamics of Highly Flexible Flying Wings," *Journal of Aircraft*, Vol. 43, No. 6, 2006, pp. 1791–1798.

[23] Shearer, C. M. and Cesnik, C. E., "Nonlinear Flight Dynamics of Very Flexible Aircraft," *Journal of Aircraft*, Vol. 44, No. 5, 2007, pp. 1528–1545.

[24] Su, W. and Cesnik, C. E. S., "Nonlinear Aeroelasticity of a Very Flexible Blended-Wing-Body Aircraft," *Journal of Aircraft*, Vol. 47, No. 5, 2010, pp. 1539–1553.

[25] Baluch, H. A. and van Tooren, M., "Modified Inertially Coupled Equations of Motion for Flexible Aircraft with Coupled Vibrations," *Journal of Aircraft*, Vol. 46, No. 1, 2009, pp. 107–115.

[26] Grossman, B., Strauch, G., Eppard, W. H., Gurdal, Z., and Haftka, R. T., "Integrated Aerodynamic/Structural Design of a Sailplane Wing," *Journal of Aircraft*, Vol. 25, No. 9, 1988, pp. 855–560.

[27] Chittick, I. R. and Martins, J. R. R. A., "An asymmetric suboptimization approach to aerostructural optimization," *Optimization and Engineering*, Vol. 10, No. 1, 2009, pp. 133–152.

[28] Anderson, M. R. and Mason, W. H., "An MDO Approach to Control-Configured-Vehicle Design," *6th AIAA/NASA/ISSMO Symposium on Multidisciplinary Analysis and Optimization*, Bellevue, WA, 1996, pp. 734–743.

[29] Perez, R. E., Liu, H. H., and Behdinan, K., "Multidisciplinary Optimization Framework for Control-Configuration Integration in Aircraft Conceptual Design," *Journal of Aircraft*, Vol. 43, No. 6, 2006, pp. 1937–1948.

[30] Noll, T. E., Ishmael, S. D., Henwood, B., Perez-Davis, M. E., Tiffany, G. C., Madura, J., Gaier, M., Brown, J. M., and Wierzbanowski, T., "Technical Findings, Lessons Learned, and Recommendations Resulting from the Helios Prototype Vehicle Mishap," Tech. Rep. 20070022260, NASA, 2007.

[31] Haghighat, S., Liu, H. H. T., and Martins, J. R. R. A., "Gust Load Alleviation Using Model Predictive Control for Large Aspect Ratio UAV Wings," *Canadian Aeronautics and Space Institute Annual General Meeting*, Ottawa, Canada, May 2009.

[32] Haghighat, S., Liu, H. H. T., and Martins, J. R. R. A., "Application of Model Predictive Control to Gust Loads Alleviation Systems," *AIAA Atmospheric Flight Mechanics*, Chicago, AIAA 2009–5929, 2009.

[33] Haghighat, S., Martins, J. R. R. A., and Liu, H. H. T., "Integrating an Active Control System with the Structural Design of a Flexible Wing Using Multidisciplinary Optimization," *International Forum on Aeroelasticity and Structural Dynamics*, Seattle, WA, June 2009.

[34] Martins, J. R. R. A., Alonso, J. J., and Reuther, J. J., "A Coupled-Adjoint Sensitivity Analysis Method for High-Fidelity Aero-Structural Design," *Optimization and Engineering*, Vol. 6, No. 1, March 2005, pp. 33–62.

[35] Karpel, M., "Procedures and Models for Aeroservoelastic Analysis and Design," *Journal of Applied Mathematics and Mechanics (ZAMM)*, Vol. 81, No. 9, 2001, pp. 579–592.

[36] Etkin, B., *Dynamics of Atmospheric Flight*, Wiley, 1972.

[37] Nelson, R. C., *Flight Stability and Automatic Control*, McGraw-Hill, 2nd ed., 1998.

[38] Meirovitch, L., *Methods of Analytical Dynamics*, McGraw-Hill, 1970.

[39] Meirovitch, L., "Hybrid State Equations of Motion for Flexible Bodies in Terms of Quasi-Coordinates," *Journal of Guidance, Control and Dynamics*, Vol. 14, No. 5, 1990, pp. 1008–1013.

[40] Martins, J. R. R. A., Sturdza, P., and Alonso, J. J., "The Complex-Step Derivative Approximation," *ACM Transactions on Mathematical Software*, Vol. 29, No. 3, 2003, pp. 245–262.

[41] Paz, M. and Leight, W., *Structural Dynamics, Theory and Computation*, Kluwer Academic Publisher, 2004.

[42] Silva, W. A., "Application of Nonlinear Systems Theory to Transonic Unsteady Aerodynmic Responses," *Journal of Aircraft*, Vol. 30, No. 5, Sept. – Oct. 1993, pp. 660–668.

[43] Silva, W. A., *Discrete-Time Linear and Nonlinear Aerodynamic Impulse Responses for Efficient CFD Analysis*, Ph.D. thesis, College of William and Mary in Virginia, 1997.

[44] Raveh, D. E. and Mavris, D. N., "Reduced-Order Models Based on CFD Impulse and Step Responses," *42nd AIAA/ASME/ASCE/AHS/ASC Structures, Structural Dynamics, and Materials Conference*, Seattle, WA, April 2001, AIAA 2001–1527.

[45] Silva, W. A. and Bartels, R. E., "Development of Reduced-Order Models for Aeroelastic Analysis and Flutter Prediction usnig the CFL3Dv6.0 Code," *Journal of Fliuds and Structures*, Vol. 19, No. 6, July 2004, pp. 729–745.

[46] Lucia, D. J., Beran, P. S., and Silva, W. A., "Reduced-Order modeling: New Approaches for Computational Physics," *Progress in Aerospace Sciences*, Vol. 40, No. 1–2, February 2004, pp. 51 – 117.

[47] Shearer, C. M. and Cesnik, C. E. S., "Trajectory Control for Very Flexible Aircraft," *Journal of Guidance, Control, and Dynamics*, Vol. 31, No. 2, 2008, pp. 340–357.

[48] Sobieszczanski-Sobieski, J., "A Technique for Locating Function Roots and for Satisfying Equality Constraints in Optimization," *Structural Optimization*, Vol. 4, No. 3–4, 1992, pp. 241–243.

[49] Poon, N. M. K. and Martins, J. R. R. A., "An Adaptive Approach to Constraint Aggregation Using Adjoint Sensitivity Analysis," *Structures and Multidisciplinary Optimization*, Vol. 30, No. 1, 2007, pp. 61–73.

[50] Perez, R. E. and Behdinan, K., *Swarm Intelligence: Focus on Ant and Particle Swarm Optimization*, chap. Particle Swarm Optimization in Structural Design, Itech Education and Publishing, Vienna, Austria, 2007, pp. 532–553.